American Mineralogist, Volume 70, pages 1211–1216, 1985

Compositional variation of naturally occurring rhoenite

A. DANA JOHNSTON

Division of Geological and Planetary Sciences
California Institute of Technology, 170–25
Pasadena, California, 91125

AND JAMES H. STOUT

Department of Geology and Geophysics,
University of Minnesota, Minneapolis, Minnesota 55455

Abstract

New electron microprobe analyses of rhoenite from an exceptionally oxidized alkali gabbro from Kauai, Hawaii are presented which greatly expand the range in composition known for this mineral. The Kauai rhoenites contain more abundant Mg, $^{IV}Fe^{3+}$, $^{VI}Fe^{3+}$, and Na, and less abundant Fe^{2+}, ^{VIII}Ca, and Ti than any previously reported terrestrial example. The abundances of Si and ^{IV}Al are among the lowest and highest, respectively, yet reported. These analyses are compared to all other available rhoenite analyses and a representative set of aenigmatite analyses. The twelve-dimensional rhoenite composition space is defined with aenigmatite as an additive component and a set of eight linearly independent simple- and coupled-ionic exchange components.

Introduction

Rhoenite is a relatively uncommon mineral typically found as a minor constituent of undersaturated alkaline igneous rocks. A review of the literature on rhoenite occurrences from its original description by Soellner (1907) from the Rhön district, Germany, through 1970 was presented by Cameron et al. (1970). More recently, rhoenite was reported from the Allende meteorite (Fuchs, 1971), from a metamorphosed basalt-limestone contact on Reunion Island (Havette et al., 1982), and from undersaturated alkaline lavas from France (Magonthier and Velde, 1976) and Antarctica and New Zealand (Kyle and Price, 1975).

The structure of rhoenite (triclinic, $P\bar{1}$) was determined by Walenta (1969) and discussed with respect to that of aenigmatite, with which it is isostructural, by Deer et al. (1978). The general formula of rhoenite, $X_2Y_6Z_6O_{20}$, was originally deduced by analogy with aenigmatite by Kelsey and McKie (1964). In this formula, X = Na, Ca, and K; Y = Fe^{2+}, Mg, Fe^{3+}, Al, Ti, Mn, and Ca; and Z = Si, Al, and Fe^{3+}.

Relatively little is known about the range in composition exhibited by naturally occurring rhoenite as fewer than 25 analyses have thus far been published. In this paper we present new electron microprobe analyses of rhoenite from an exceptionally oxidized alkali gabbro from Kauai, Hawaii. These data greatly expand the known compositional range of rhoenite and, when combined with previously published analyses, provide an opportunity to identify substitutions by which the observed displacements through composition space may be achieved.

The samples come from a composite, subvolcanic plug located just north of the town of Kalaheo, near the south coast of Kauai, Hawaii. The petrography and mineral chemistry of these samples and their isotope and trace element geochemistry and probable origin have been discussed by Johnston and Stout (1984) and Johnston et al. (1985). Although field exposures are poor, it is likely that the plug consists of a central core of ijolite that has a relatively low oxidation state (near Ni–NiO) and a highly oxidized (>M–H) border facies consisting of abundant mantle-derived xenoliths within a composite matrix of alkali picrite and rhoenite-bearing alkali gabbro. Both of the latter lithologies have exceptionally high Fe^{3+}/Fe^{2+} atomic ratios (~9.0) and correspondingly unusual mineral assemblages (Johnston and Stout, 1984).

The alkali gabbro has a prophyritic texture and a mineral assemblage rich in Fe^{3+} and Mg that clearly attests to its crystallization from a highly oxidized melt. This assemblage consists of ferrian salite, magnesioferrite, and nearly pure forsterite phenocrysts, microphenocrysts of kaersutite, apatite and rhoenite, and a quench-textured groundmass of oligoclase, kennedyite, and magnesian hematite. The rhoenite occurs as skeletal grains with well developed crystal faces (Fig. 1) exhibiting very strong absorption and pronounced pleochroism (olive-brown, red-brown, black). These grains are generally elongate with cross-sectional diameters of approximately 0.1–0.2 mm and lengths of 2–6 mm.

Methods

All analyses reported in Table 1 were performed by JHS at the University of Bergen, Norway using a fully automated ARL SEMQ

0003–004X/85/1112–1211$02.00

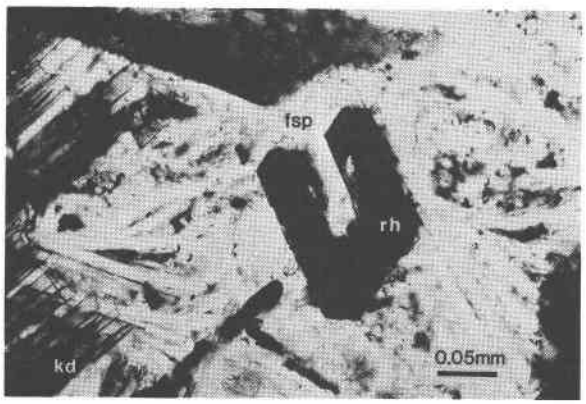

Fig. 1. Photomicrograph illustrating skeletal form and well-developed crystal faces of rhoenite from the Kauai alkali gabbro. Also visible are blades of kennedyite (kd) and oligoclase (fsp).

electron microprobe. Operating conditions were 15 kV accelerating potential, 10 nA beam current, ~2 μm beam diameter, and counting times of 40 s on peaks and 4 s on backgrounds. Standards consisted of wollastonite (Ca, Si), jadeite (Na), orthoclase (K), rutile (Ti), synthetic oxides (Mg, Al, Mn), and pure Fe metal.

Table 1. Electron microprobe analyses of rhoenite from Kauai

	1	2	3	4	5	
SiO_2	25.95	30.00	25.10	30.74	27.90	
TiO_2	10.03	5.08	6.88	5.73	9.06	
Al_2O_3	13.12	12.29	14.75	12.64	13.48	
FeO*	19.17	19.27	20.94	16.00	17.64	
MgO	16.81	18.05	17.14	19.50	17.78	
CaO	8.60	9.18	10.30	8.36	9.15	
MnO	0.22	0.36	0.29	0.26	0.19	
Na_2O	2.82	2.63	1.91	3.08	2.89	
K_2O	0.02	n.d.	0.01	0.06	n.d.	
Σ	97.29	96.87	97.35	96.38	98.11	
FeO**	3.68	2.18	1.44	0.37	2.86	
Fe_2O_3**	17.21	18.99	21.66	17.37	16.42	
Σ**	99.01	98.77	99.51	98.12	99.75	
14 cations and 20 oxygens						
Si	3.45	3.94	3.33	4.01	3.64	4-fold
Al	2.05	1.91	2.30	1.94	2.07	
Fe^{3+}	0.50	0.15	0.37	0.05	0.29	
Fe^{3+}	1.27	1.73	1.79	1.65	1.31	6-fold
Fe^{2+}	0.42	0.24	0.16	0.04	0.31	
Mg	3.33	3.53	3.38	3.78	3.45	
Ti	1.00	0.50	0.69	0.56	0.89	
Mn	0.02	0.04	0.03	0.03	0.02	
Ca	1.23	1.29	1.46	1.16	1.28	8-fold
Na	0.73	0.67	0.49	0.77	0.73	
K	0.00	n.d.	0.00	0.01	n.d.	

*total Fe as FeO; **based on calculated Fe^{2+} and Fe^{3+}; n.d.: not determined

Data reduction and ZAF corrections were performed on line using the MAGIC IV computer program (Colby, 1968). Typical standard deviations of determined weight percent oxides are <1% of the amount present for oxides present in excess of 5 wt.%, 2–3% for oxides in the range 1–5 wt.%, and 10–20% of the amount present for oxides present in amounts less than 1 wt.%. All iron was determined as FeO.

Ferric iron was calculated by assuming Fe to be the only element present with more than one valence state and by assuming rhoenite stoichiometry of 14 cations and 20 oxygens. The cation sum of each analysis was normalized to 14, and their oxygen equivalents were calculated. Ferric iron was then calculated by $Fe^{3+} = 2(20 - \text{calculated } \# \text{ oxygens})$ where the calculated number of oxygens treats all iron as ferrous (Finger, 1971). All literature analyses appearing in Figure 2 for which wet chemical determinations of Fe_2O_3 were lacking were recalculated following this procedure before plotting.

Cations were assigned to the various structural sites according to the following scheme. All Si and sufficient Al to bring the total to 6.0 were assigned to be tetrahedrally coordinated Z-sites. If there was insufficient Al, Fe^{3+} was added to (Si + Al) to bring the total to 6.0. Any remaining Al and Fe^{3+}, together with Fe^{2+}, Mg, Mn, Ti, and sufficient Ca to bring the total to 6.0 were assigned to the octahedral Y-sites. The remaining Ca and all Na and K were assigned to the 8-fold X-sites.

Results

Selected rhoenite analyses from six Kauai samples, chosen to illustrate the range in composition we observed, are given in Table 1. These data, together with other Kauai rhoenite analyses not appearing in Table 1 (26 analyses total, available from ADJ) were recalculated to structural formulae and plotted as the shaded pattern in Figure 2. Also appearing in Figure 2 are recalculated structural formulae from all other published rhoenite analyses of which we are aware (21 analyses) as well as a representative set of aenigmatite analyses (44 analyses) for comparison. The sources of these analyses are marked with an asterisk in the references. In addition to these, all rhoenite and aenigmatite analysis compiled by Deer et al. (1978, except rhoenite analysis #1, p. 656, which is clearly inferior) are included in Figure 2. Octahedrally coordinated Mn and Ca and 8-fold K were not plotted because they show virtually no variability and seldom exceed 0.2, 0.1 and 0.1 cations per formula unit, respectively. The only exception is the very unusual rhoenite composition reported from the Allende meteorite (Fuchs, 1971) which contains 0.44 ^{VI}Ca per formula unit. This analysis is also noteworthy because stoichiometric and charge balance constraints require that ~28 percent of the Ti be present in the +3 valence state, consistent with its meteoritic paragenesis.

A number of interesting features are illustrated in Figure 2. First, it is clear that the Kauai rhoenite analyses (Table 1, Fig. 2: shaded pattern) greatly expand the known range in composition of naturally occurring rhoenite. This is particularly the case for Mg, $^{IV}Fe^{3+}$, $^{VI}Fe^{3+}$, and Na which are more abundant and ^{VIII}Ca and Ti which are less abundant than in any previously reported example. Moreover, the Kauai rhoenites contain less Fe^{2+} than any other terrestrial example, the only comparable analysis being that

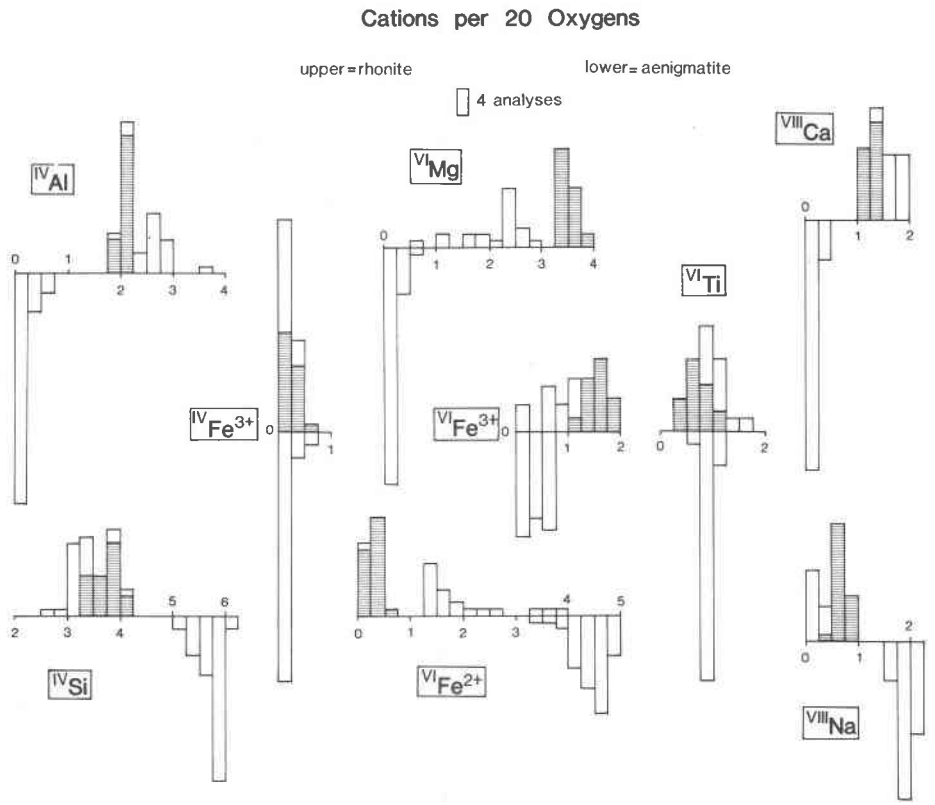

Fig. 2. Structural formula histograms containing 26 rhoenite analyses from this study (shaded pattern above horizontal axes), all previously published rhoenite analyses (unshaded, above horizontal axes), and a representative set of aenigmatite analyses (below horizontal axes). Note that the data from this study greatly expand the known range of rhoenite compositional variation. Also note the gaps in composition between rhoenite and aenigmatite (Si, ^{IV}Al, Na, ^{VII}Ca).

from the Allende meteorite (Fuchs, 1971). Furthermore, the abundances of Si and ^{IV}Al in the Kauai rhoenites are among the highest and lowest, respectively, yet reported. The reader is cautioned, however, not to ascribe too much statistical significance to the peak shapes of the rhoenite histograms as certain data sets, notably the Kauai data, are over-represented.

Also clear from Figure 2 is the remarkably restricted range in composition of naturally occurring aenigmatite. The only significant departures from its ideal formula ($Na_2Fe_5^{2+}TiSi_6O_{20}$) are due to limited substitution of Al for Si in tetrahedral sites, Fe^{3+} for Fe^{2+} in octahedral sites, and Ca for Na in 8-fold sites.

Considerable discussion has been devoted to the possibility that rhoenite and aenigmatite may form an isomorphous series (e.g., Cameron et al., 1970, Grunhagen and Seck, 1975). Although rhoenite is isostructural with aenigmatite (and sapphirine, serendibite and krinovite, Deer et al., 1978), no evidence of continuous compositional variation between them has yet been presented. Indeed, the discontinuously zoned and intergrown rhoenite and aenigmatite reported by Yagi (1953, p. 786 and Plate 4), provide compelling evidence for the existence of a miscibility gap between them. The data plotted in Figure 2 appear to corroborate this suggestion. Although there is considerable overlap between rhoenite and aenigmatite in some cations on given sites ($^{IV}Fe^{3+}$, $^{VI}Fe^{3+}$, Ti), there are distinct gaps in composition for most others, notably ^{IV}Al, Si, ^{VIII}Ca, and Na (Figs. 2 and 3). However, in terms of tetrahedral and 8-fold site occupancies, the Kauai rhoenites approach ideal aenigmatite more closely than any previously reported (Figs. 2 and 3), but whereas Fe^{2+} is the dominant octahedral cation in aenigmatite, Mg is dominant in the Kauai rhoenites. Thus, the Kauai rhoenites may be regarded as showing substantial solubility toward a hypothetical Mg-aenigmatite component ($Na_2Mg_5TiSi_6O_{20}$). Solubility toward true aenigmatite, however, is very limited in the Kauai rhoenites due to their exceptionally low octahedral Fe^{2+} contents.

Rhoenite composition space

In considering the range in composition of naturally occurring rhoenite, we have found it useful to describe the analyses with respect to ideal aenigmatite, as an additive component, with a set of exchange components (see Thompson, 1982 for a discussion of this method). This approach has the advantage over the more conventional use of only additive components, that the exchange compo-

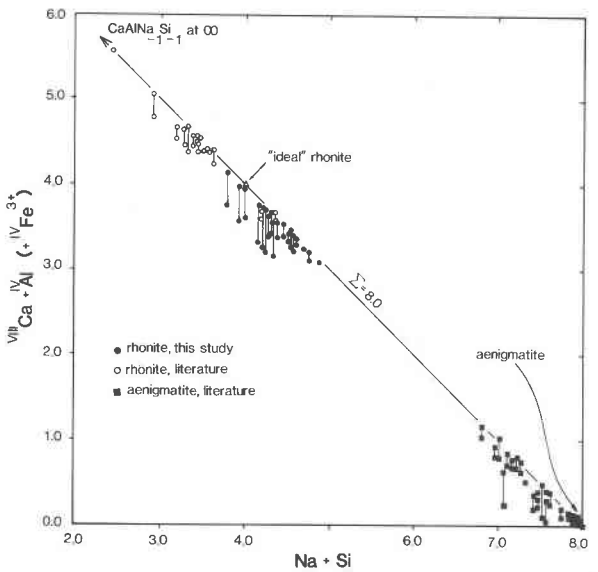

Fig. 3. Na + Si versus ^{VIII}Ca + ^{IV}Al (lower point) and ^{VIII}Ca + ^{IV}Al + ^{IV}Fe^{3+} (upper point) correlation diagram for naturally occurring rhoenite and aenigmatite. Some overlapping data points have been omitted for clarity. The vertical lines connecting points reflect the extent to which Fe^{3+} replaces Si in tetrahedral sites.

nents have the form of ionic substitutions and thus bear more directly on the problem. Such components (e.g., $FeMg_{-1} = Fe \rightleftharpoons Mg$) represent operations rather than realizable chemical compositions and may be regarded as a set of vectors by which the composition space of interest may be described. The actual composition variables (e.g., $X_{FeMg_{-1}}$) represent the number of moles of each exchange component per mole of additive component required to generate the analysis of interest.

We have chosen aenigmatite as the additive component because of its relatively simple ideal formula and because it has the same stoichiometry as rhoenite. The number of additional independent exchange components required to describe a rhoenite analysis equals the number of variables minus the number of constraints. By describing each rhoenite analysis as a point in n-dimensional composition space where each of the n coordinate axes is the number of cations in a particular structural site, the number of variables considered is twelve: the amounts of Na, ^{VIII}Ca, ^{VI}Ca, Mg, Mn, Ti, Fe^{2+}, $^{VI}Fe^{3+}$, ^{VI}Al, ^{IV}Al, $^{IV}Fe^{3+}$, and Si, per 20 oxygens. The number of constraints is four, three from rhoenite stoichiometry: $^{VIII}(Na + Ca) = 2$, $^{VI}(Ca + Mg + Ti + Fe^{2+} + Mn + Fe^{3+} + Al = 6)$, $^{IV}(Al + Fe^{3+} + Si) = 6$, and one from the site-charge balance requirement. Thus, eight independent exchange components are required to specify the location of a rhoenite analysis relative to aenigmatite in the 12-dimensional composition space of interest.

A number of these exchange components may be readily identified from plots such as Figures 3, 4, and 5. In Figure 3 we have plotted (Na + Si) versus (^{VIII}Ca + ^{IV}Al) (lower point) and (^{VIII}Ca + ^{IV}Al + $^{IV}Fe^{3+}$) (upper point) for all the analyses used to construct Figure 2. The line in Figure 1 has a slope of −1.0 and represents the coupled substitution $Ca + Al \rightleftharpoons Na + Si$. Ideal rhoenite and aenigmatite plot on this line as does the exchange component $CaAlNa_{-1}Si_{-1}$ demonstrating that, in terms of tetrahedral and 8-fold coordinated site occupancies, the ideal formulae of these minerals are related by this substitution. It is noteworthy though, that three of the Kauai rhoenite analyses and all of the literature rhoenite analyses (all analyses to the upper left of ideal rhoenite, Fig. 3) contain more tetrahedral Al than can be compensated by 8-fold Ca. This excess tetrahedral Al, therefore, must be compensated by charge excess in the octahedral sites which may be introduced through the coupled substitutions $^{IV}Al + {}^{VI}Al \rightleftharpoons Si + (Fe^{2+} + Mg)$ and $^{IV}Al + {}^{VI}Fe^{3+} \rightleftharpoons Si + (Fe^{2+} + Mg)$. The lengths of the vertical lines connecting points in Figure 3 are measures of the extent to which Fe^{3+} occurs replacing Si in tetrahedral sites. The charge deficiency resulting from this substitution must also be compensated by octahedral charge excess through the coupled substitutions $^{IV}Fe^{3+} + {}^{VI}Fe^{3+} \rightleftharpoons Si + (Fe^{2+} + Mg)$ or $^{IV}Fe^{3+} + {}^{VI}Al \rightleftharpoons Si + (Fe^{2+} + Mg)$. The second of these, however, is a linear combination of the first and the two given above and thus, may be discarded.

In Figure 4, the exchange relationship $Fe^{2+} \rightleftharpoons Mg$ in rhoenite and aenigmatite is clearly shown. Considering that ideal aenigmatite is a pure Fe^{2+}-endmember, this substitution may also be regarded as one that relates rhoenite and aenigmatite. It is also clear from Figure 4 that whereas natural aenigmatites contain close to the ideal number (5.0) of divalent octahedral cations, natural rhoenites, particularly those from this study, contain considerably fewer (3.8–4.4). Moreover, the concentrations of ^{VI}Ca and Mn, which

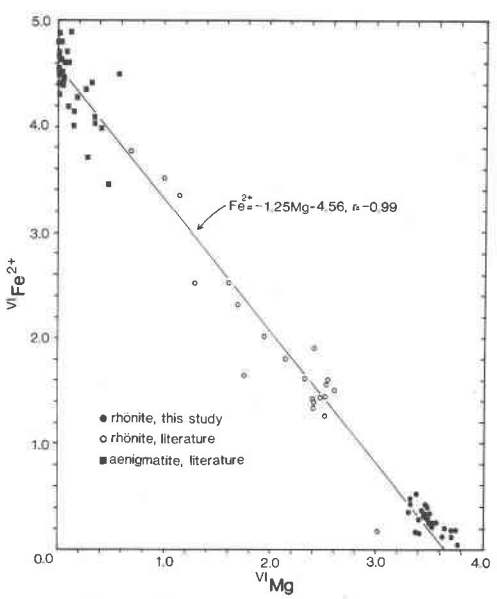

Fig. 4. Fe^{2+} versus Mg correlation diagram for naturally occurring rhoenite and aenigmatite. Note the low (Fe^{2+} + Mg) totals for most rhoenite analyses.

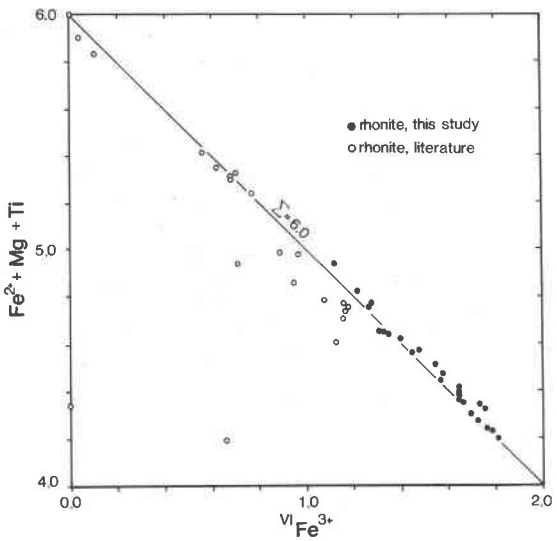

Fig. 5. $^{VI}Fe^{3+}$ versus Ti + Mg + Fe^{2+} correlation diagram for naturally occuring rhoenite. Analyses that deviate from the line contain appreciable ^{VI}Al.

may be introduced through the analogous substitutions $Fe^{2+} \rightleftharpoons {}^{VI}Ca$ and $Fe^{2+} \rightleftharpoons Mn$, are much too low to bring the total to 5.0.

This deficiency in the number of divalent octahedral cations is compensated in natural rhoenites by the introduction of octahedral Fe^{3+}. To maintain charge balance, however, Fe^{3+} must replace Ti to the same extent as it replaces divalent cations by the substitution $2^{VI}Fe^{3+} \rightleftharpoons Ti + (Fe^{2+} + Mg)$, which is plotted in Figure 5. The line drawn through the data has a slope of -1.0 and represents a constant cation sum of 6.0. All points which deviate significantly from this line represent analyses containing appreciable ^{VI}Al, introduced through one of the substitutions already discussed. In rare cases (e.g., Havette et al., 1982; Kyle and Price, 1975), natural rhoenites contain excess Ti (i.e., >1.0 Ti per 20 oxygen) which may be introduced by a substitution such as $Ti + 2(^{IV}Fe^{3+}, {}^{IV}Al) \rightleftharpoons (Fe^{2+}, Mg) + 2Si$. This exchange, however, is simply a linear combination of some of the substitutions already discussed and is therefore not considered further.

The eight independent exchange components just discussed are listed in Table 2 together with the equations by which they may be calculated from a rhoenite structural formula. These vectors all pass through aenigmatite which serves as the origin of the 12-dimensional rhoenite composition space. Through the application of some or all of these operations, the full extent of compositional variation in naturally occurring rhoenite (and aenigmatite) may be described. As an example of the application of these exchange operations, we have recalculated the analyses in Table 1 to these components and list them, in units of moles per mole of aenigmatite, in Table 2. Thus, each rhoenite analysis may be generated by mixing one mole of aenigmatite with the number of moles of each exchange component indicated in Table 2. Because the Kauai rhoenites lack ^{VI}Ca and ^{VI}Al, the components $^{VI}CaFe^{2+}_{-1}$ and $^{IV}Al^{VI}AlSi_{-1}Fe^{2+}_{-1}$ are not required for their full description. By simply subtracting one list from another, any two rhoenite analyses may be related directly by removing their common reference to aenigmatite.

Table 2. Rhoenite exchange components

	Exchange Component	Analyses from Table 1					Equation
		1	2	3	4	5	
A.	$MgFe^{2+}_{-1}$	3.33	3.53	3.38	3.78	3.45	Mg
B.	$^{VI}CaFe^{2+}_{-1}$	0.00	0.00	0.00	0.00	0.00	^{VI}Ca
C.	$MnFe^{2+}_{-1}$	0.02	0.04	0.03	0.03	0.02	Mn
D.	$^{VIII}Ca^{IV}AlNa_{-1}Si_{-1}$	1.23	1.29	1.46	1.16	1.28	^{VIII}Ca
E.	$2^{VI}Fe^{3+}Ti_{-1}Fe^{2+}_{-1}$	0.00	0.50	0.31	0.44	0.11	1-Ti
F.	$^{IV}Al^{VI}AlSi_{-1}Fe^{2+}_{-1}$	0.00	0.00	0.00	0.00	0.00	^{VI}Al
G.	$^{IV}Fe^{3+}{}^{VI}Fe^{3+}Si_{-1}Fe^{2+}_{-1}$	0.50	0.15	0.37	0.05	0.29	$^{IV}Fe^{3+}$
H.	$^{IV}Al^{VI}Fe^{3+}Si_{-1}Fe^{2+}_{-1}$	0.82	0.62	0.84	0.78	0.79	^{IV}Al-D-F

*in units of moles per mole of aenigmatite

Acknowledgments

We would like to thank the staff of the University of Bergen, and in particular, Dr. Brian Robins, for providing access to and assistance in operating their electron microprobe/SEM facility.

Financial support from the Geological Society of America (research grant 2850-81 to ADJ), from NATO (fellowship to JHS), and from the National Science Foundation (Grant EAR 7812947 to JHS) is gratefully acknowledged. Additional funding for this research was provided to ADJ in the form of a Phillips Petroleum Foundation, Inc. graduate fellowship at the Department of Geology and Geophysics, University of Minnesota. The manuscript was prepared while ADJ held a post-doctorate fellowship from the Royal Norwegian Council for Scientific and Industrial Research (NTNF).

References[1]

Boivin, par Pierre (1980) Données expérimentales preliminaires sur la stabilité de la rhönite à 1 atmosphère. Application aux gisements naturels. Bulletin de Mineralogie, 103, 491–502.*

Bryan, W. B. and Stevens, N. C. (1973) Holoycrystalline pantellerite from Mt. Ngun-Ngun, Glass House Mountains, Queensland, Australia. American Journal of Science, 273, 947–957.*

Cameron, K. L., Carman, M. F., and Butler, J. C. (1970) Rhönite from Big Bend National Park, Texas. American Mineralogist, 55, 864–874.*

Colby, J. W. (1968) MAGIC IV—a computer program for quantitative electron microprobe analysis. Advances in X-ray Analysis, 11, 287–305.

Deer, W. A., Howie, R. A., and Zussman, J. (1978) Rock-Forming Minerals, Vol. 2a, Single Chain Silicates. Wiley, New York.

Fuchs, L. H. (1971) Occurrence of wollastonite, rhönite, and andradite in the *Allende* meteorite. American Mineralogist, 56, 2053–2068.*

Havette, par Andree, Clochiatti, R., Nativel, P., and Mantaggioni, L. (1982) Une paragenese inhabituelle a fassaite, melilite et rhönite dans un basalte alcalin contamine au contact d'un recif corallien (Saint-Leu, Ile de la Reunion). Bulletin de Mineralogie, 105, 364–375.*

[1] Asterisk denotes reference used in compiling Figure 2.

Johnston, A. D. and Stout, J. H. (1984) A highly oxidized ferrian salite-, kennnedyite-, forsterite-, and rhönite-bearing alkali gabbro from Kauai, Hawaii and its mantle xenoliths. American Mineralogist, 69, 57–68.

Johnston, A. D., Stout, J. H. and Murthy, V. R. M. (1985) Geochemistry and origin of some unusually oxidized alkaline rocks from Kauai, Hawaii. Journal of Volcanology and Geothermal Research, 25, 225–248.

Jones, A. P. (1984) Mafic silicates from the nepheline syenites of the Motzfeldt centre, South Greenland. Mineralogical Magazine, 48, 1–12.*

Kelsey, C. H. and McKie, D. (1964) The unit-cell of aenigmatite. Mineralogical Magazine, 33, 986–1001.*

Kyle, P. R. and Price, R. C. (1975) Occurrences of rhönite in alkalic lavas of the McMurdo Volcanic Group, Antarctica, and Dunedin Volcano, New Zealand. American Mineralogist, 60, 722–725.*

Larsen, L. M. (1977) Aenigmatites from the Ilimaussaq intrusion, south Greenland: chemistry and petrological implications. Lithos, 10, 257–270.*

Magonthier, M. C. and Velde, D. (1976) Mineralogy and petrology of some Tertiary leucite-rhönite basanites from central France. Mineralogical Magazine, 40, 817–826.*

Soellner, J. (1907) Ueber Rhönit, ein neues änigmatitähnliches Mineral und über die Verbreitung desselben in basaltischen Gesteinen. Neues Jahrbuch für Mineralogie, 24, 475–547.*

Thompson, J. B., Jr. (1982) Composition space: an algebraic and geometric approach. In J. M. Ferry, Ed., Characterization of Metamorphism through Mineral Equilibria. Mineralogical Society of America Reviews in Mineralogy, 10, 1–31.

Walenta, von Kurt (1969) Zur kristallographie des Rhönits. Zeitschrift für Kristallographie, 130S, 214–230.

Yagi, K. (1953) Petrochemical studies on the alkalic rocks of the Morutu District, Sakhalin. Bulletin of the Geological Society of America, 64, 769–810.

Manuscript received, December 14, 1984;
accepted for publication, July 22, 1985.